DEVELOPMENT OF A THERMAL-MECHANICAL-MATERIAL BEHAVIOR ANALYSIS CODE FOR THE DISPERSION-PLATE-TYPE FUEL

Yingwei Wu*, Qing Lu, Yangbin Deng
School of Nuclear Science and Technology, State Key Laboratory of Multiphase Flow in Power Engineering, Xi'an Jiaotong University
Xi'an 710049, China
wyw810@mail.xjtu.edu.cn; yb.Deng.86 @stu.xjtu.edu.cn

Dalin Zhang, Wenxi Tian, Suizheng Qiu, Guanghui Su
Department of Nuclear Engineering
Xi'an Jiaotong University
Xi'an 710049, China
dlzhang@mail.xjtu.edu.cn; wxtian@mail.xjtu.edu.cn; szqiu@mail.xjtu.edu.cn; ghsu@mail.xjtu.edu.cn

ABSTRACT

In this study, the relevant thermal-hydraulic, mechanic-material and burnup effect calculation models were established. On the basis of these mathematic and physic models, a thermal-mechanic-material coupling analysis code for a dispersion-plate-type fuel assembly was independently developed with the consideration of the burnup effects. The coupling program was applied to perform the thermal-mechanical-material behavior analysis of a dispersion-plate-type fuel assembly. Major physical parameters at different burnup stages were well predicted, including flux distribution, temperature profile, Mises stress and mechanic deformations. The result shows that geometric sizes of flow channels are the key parameters determining the coolant flux distribution and the temperature profile of the edge plate presents substantial asymmetry as a result of asymmetric heat transfer caused by the asymmetric geometry. Furthermore, the equivalent stress of base material increased rapidly with burnup because of the thermal expansion and burnup effects, which resulted in substantial plastic deformation and mechanical damage. In addition, the mechanism and process of blistering was investigated for blistering prediction. The result shows that due to the increasing fission gas pressure and the deteriorating yield stress of the cladding, fuel plate blistering may happen when the burnup depth up to a certain value and fuel plate will finally fall into failure as a result of over plastic deformation.

Key Words: Dispersion-plate-type fuel, thermal-mechanic-material analysis code, asymmetric heat transfer, blistering

1 INTRODUCTION

In the past few decades, much attention has been devoted to the study on commercial fuel rods and many relevant fuel behavior analysis codes were developed, such as FRAPCON [1] and FRAPTRAN [2]. However, the different fuel material and geometric construction of dispersion-plate-type fuel result in totally different physical phenomena and failure modes. Although much research has been conducted on fuel plates, few researchers have considered the thermal-mechanical-material behavior coupling analysis with the consideration of burnup effects. Furthermore, the previous studies on blistering failure were

mainly focused on the experimental research to determine the threshold temperature [3, 4], but few literatures introduced the numerical calculation of blistering prediction.

So in this study, attention was devoted to develop a dispersion-type fuel behavior analysis code, which can perform the thermal-mechanical-material coupling calculation at different burnup stages and provide the blistering prediction. Based on this code, the study of coolant flux distribution, asymmetric heat transfer, matrix damage and blistering failure were conducted. Furthermore, since this code was developed for a total plate-type assembly, it might be modified to simulate assembly bending and torsion in the future.

2 PHYSICAL MODEL

2.1 Geometric Model

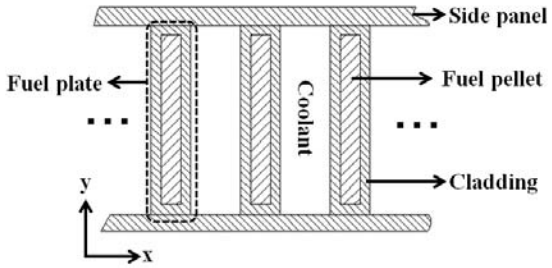

Figure 1. Vertical view of a fuel assembly

As shown in figure 1, a plate-type fuel assembly is composed of several parallel fuel plates and two side panels for fixation and coolant flow in rectangular channels. A fuel plate consists of the fuel pellet and claddings on both sides. Side panels and claddings are made of Zr while the dispersion pellet was made by UO_2 fuel grains and the Zr matrix.

2.2 Thermal-hydraulic Models

Table I presents the convective heat transfer and pressure drop calculation models. The consideration of suitability for small rectangular channels accounts for the selection of these specific correlations in this study. Other thermal-hydraulic models, such as coolant temperature calculation, heat conductivity of fuel plates, are relatively simple and will not introduce in this paper.

Table I. Major thermal-hydraulic calculation models

Model	Formula	
Convective heat transfer	Single phase: Petukhov [5] correlation	$\begin{cases} Nu = \dfrac{f\,\mathrm{Re}\,\mathrm{Pr}}{8X}\left(\dfrac{\mu_b}{\mu_w}\right)^{0.11} \\ f = \left(1.82\log \mathrm{Re} - 1.64\right)^{-2} \\ X = 1.07 + 12.7\left(\mathrm{Pr}^{2/3} - 1.0\right)\left(\dfrac{f}{8}\right)^{0.5} \end{cases}$
	Subcooled boiling: Bergles-Rohsenow [6] correlation	$\begin{cases} q_{ONB} = Nu\dfrac{k_l}{De}\left(T_{WONB} - T_b\right) \\ T_{WONB} - t_s = 0.5556\left[\dfrac{q_{ONB}}{1082\,p^{1.156}}\right]^{0.463P^{0.0234}} \end{cases}$

	Saturation boiling: Chen [7] correlation	$h = 0.023F\left[\frac{G(1.0-x)De}{\mu_f}\right]^{0.8}\left[\frac{\mu Cp}{k}\right]_f^{0.4}\left(\frac{k_f}{De}\right)+ 0.00122S\left[\frac{k_f^{0.79}C_{pf}^{0.45}\rho_f^{0.49}}{\sigma^{0.5}\mu_f^{0.29}h_{fg}^{0.24}\rho_g^{0.24}}\right](T_w-T_S)^{0.24}(p_w-p_s)^{0.75}$
Pressure drop calculation	Gravitational pressure drop	$\Delta P_{el}=\int_{z_1}^{z_2}\left(\alpha\rho_{gs}+(1-\alpha)\rho_{fs}\right)\cdot g\sin(\theta)dl$
	Friction pressure drop	$\begin{cases}\Delta P_f = f\frac{L}{De}\frac{\rho V^2}{2}\\ f=\frac{0.184}{\mathrm{Re}^{0.2}}\\ \Phi_{lo}^2=\left[1.0+x\left(\frac{v_g-v_f}{v_f}\right)\right]\left[1.0+x\left(\frac{\mu_f-\mu_g}{\mu_g}\right)\right]^{-.025}\end{cases}$
	Acceleration pressure drop	Single phase: $\Delta p_a = G(V_2-V_1)=G^2(v_2-v_1)$ Two phase: $\begin{cases}\Delta p_a = r_2G^2v_l\\ r_2=\frac{\rho_l x_{out}^2}{\alpha\rho_v}+\frac{1}{\rho_l}\left[\frac{(1-x_{out})^2}{1-\alpha}-1\right]\end{cases}$

2.3 Fission Gas Release and Gas Pressure Calculation

Fission gas release should be investigated for the prediction of blistering. Fission gas release, involving many mechanisms, can be divided into two patterns: the athermal regime and the thermally-activated regime. Due to the much lower fuel temperature than that of solid fuel, the thermally-activated gas release is neglected in this study. The following formula of fission gas release was used in this study:

$$\begin{cases} F=\begin{cases}5\times10^{-4}Bu+C; & F<0.1\\ 0.05; & F>0.1\end{cases}\\ C=\begin{cases}0; Bu<40\\ 0.001\times(Bu-40); & Bu>40\end{cases}\end{cases} \quad (1)$$

where F represents the fission gas release fraction and Bu represents the burnup.

The volume available to the fission gas, including cracks and intergranular space is the indispensable parameter for gas pressure calculation. However, it's quite complex to predict the accurate volume value. At high burnup stage, we assumed that: 1) all fuel matrixes were broken; 2) fission gas release fraction up to 10% (the maximum value); 3) the gas pressure up to 70MPa. Based on that, the largest free volume for fission gas can be calculated. Multiplying the maximum value by the volume fraction of damaged matrix and then the approximate available volume for gas at any moment can be obtained. It can be claimed that the matrix was damaged if the plastic deformation occurred and relevant elastic-plastic models will be introduced in next section.

2.4 Elastic-plastic Calculation Model

2.4.1 Plane strain problem

As for a fuel plate, the size in height direction (z) is much larger than sizes in another two directions (x and y), so the elastic calculation of the plate can be regard as the typical plane strain problem. The fundamental equations for solving the plane strain problem, including the equilibrium equation, the geometric equation and the physical equation, are presented as follows:

Equilibrium equation:

$$\begin{cases} \dfrac{\partial \sigma_x}{\partial x} + \dfrac{\partial \tau_{yx}}{\partial y} = 0 \\ \dfrac{\partial \tau_{xy}}{\partial x} + \dfrac{\partial \sigma_y}{\partial y} = 0 \end{cases} \tag{2}$$

Geometric equation:

$$\begin{cases} \varepsilon_x = \dfrac{\partial u}{\partial x} \\ \varepsilon_y = \dfrac{\partial v}{\partial y} \\ \gamma_{xy} = \dfrac{\partial v}{\partial x} + \dfrac{\partial u}{\partial y} \end{cases} \tag{3}$$

Physical equation:

$$\begin{cases} \varepsilon_x = \dfrac{1}{E}\left[\sigma_x - \mu(\sigma_y + \sigma_z)\right] + \varepsilon_x^{'} \\ \varepsilon_y = \dfrac{1}{E}\left[\sigma_y - \mu(\sigma_z + \sigma_x)\right] + \varepsilon_y^{'} \\ \varepsilon_z = \dfrac{1}{E}\left[\sigma_z - \mu(\sigma_x + \sigma_y)\right] + \varepsilon_z^{'} = 0 \\ \gamma_{xy} = \dfrac{1}{G}\tau_{xy} \end{cases} \tag{4}$$

where u, v represent displacements in x, y direction and E, G represent Young modulus and shear modulus. $\varepsilon^{'}$ represents the intrinsic strain including the thermal expansion, irradiate swelling, fuel densification, plastic strain and plastic strain increment:

$$\varepsilon^{'} = \varepsilon_{thermal} + \varepsilon_{swelling} + \varepsilon_{densificaiton} + \varepsilon_{plastic} + \Delta\varepsilon_{plastic} \tag{5}$$

2.4.2 Simplify of plane strain problem

To solve the plane strain problem, the finite element method is indispensable. However, considered the size in x direction is much smaller than that in y direction and the mechanical deformation in y

direction is restricted by side panels, the strain in *y* direction could be supposed as zero ($\varepsilon_y = 0$) and the physical equation can be simplified as following:

$$\begin{cases} \varepsilon_x = \dfrac{1}{E}\left[\sigma_x - \mu(\sigma_y + \sigma_z)\right] + \varepsilon_x^{'} \\ \varepsilon_y = \dfrac{1}{E}\left[\sigma_y - \mu(\sigma_z + \sigma_x)\right] + \varepsilon_y^{'} = 0 \\ \varepsilon_z = \dfrac{1}{E}\left[\sigma_z - \mu(\sigma_x + \sigma_y)\right] + \varepsilon_z^{'} = 0 \end{cases} \tag{6}$$

In addition, the intrinsic strains in both *y* and *z* directions were translated into strain in *x* direction with the compression of fixing device in *y* and *z* direction. So the total strain in *x* direction can be expressed as the following formula:

$$\varepsilon_x = \varepsilon_x^{'} + \mu\left(\varepsilon_y^{'} + \varepsilon_z^{'}\right) - \frac{P_{coolant}}{E} \tag{7}$$

where μ is the Poisson ratio and $P_{coolant}$ is the coolant pressure acting on the plate.

The equation set consisting formula (6) and (7) formula is a closed four order algebraic equation set and can solved by gauss iterative method. The above simplify greatly reduced the difficulty of code development.

2.4.3 Elastic-plastic transition and calculation

According to the Von Mises yield criteria, the material deformation will enter into plastic stage from elastic stage when the equivalent stress up to the yield stress. The Mises stress (equivalent stress) can be calculated by the following equation:

$$\sigma_e = \frac{1}{\sqrt{2}}\sqrt{(\sigma_1 - \sigma_2)^2 + (\sigma_2 - \sigma_3)^2 + (\sigma_3 - \sigma_1)^2} \tag{8}$$

where σ_e represents equivalent stress and σ_1, σ_2, σ_3 represent stress component in three directions.

Once the material was yielded, the linear elasticity theory is out of application and the Prandtl-Reuss incremental theory [8, 9] was used to obtain the strain and stress in plastic stage. In the incremental theory, the equivalent plastic strain is defined as the sum of all increments $d\varepsilon^p$, which is related to the individual plastic strain components by:

$$d\varepsilon^p = \frac{\sqrt{2}}{3}\left[\left(d\varepsilon_1^p - d\varepsilon_2^p\right)^2 + \left(d\varepsilon_2^p - d\varepsilon_3^p\right)^2 + \left(d\varepsilon_3^p - d\varepsilon_1^p\right)^2\right]^{0.5} \tag{9}$$

where the $d\varepsilon_i^p$ (*i*=1, 2, and3) are the plastic strain components in principle coordinates.

The relationship between the magnitudes of the plastic strain increments and the effective plastic strain increment is provided by Prandtl-Reuss flow rule:

$$\begin{cases} d\varepsilon_i^p = \dfrac{3d\varepsilon^p}{2\sigma_e} s_i, \quad i = 1,2,3 \\ s_i = \sigma_i - \dfrac{1}{3}\left(\sigma_1 + \sigma_2 + \sigma_3\right) \end{cases} \tag{10}$$

According to the Prandtl-Reuss incremental theory, the elastic and plastic calculation should be coupled until converged and the coupling calculation flow diagram is presented in figure 2.

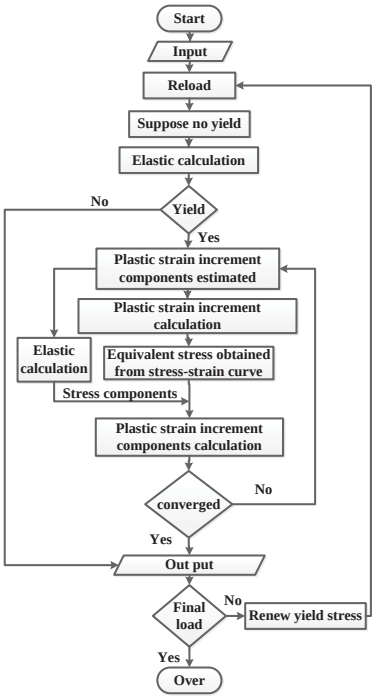

Figure 2. Vertical view of a fuel assembly

2.5 Material Equivalent Property Model

Equivalent properties of the matrix diffusion pellet, including thermal conductivity, thermal expansion rate and elastic modulus (Young modulus, shear modulus, Poisson ratio and bulk modulus) should be calculated for thermal or mechanical calculation. These equivalent properties were obtained by the equations published in the existing literatures, where the equivalent property was expressed as the function of property values and volume contents of material components.

2.5.1 Equivalent thermal conductivity:

Maxwell [10]:

$$k_{eff} = \frac{k_2\left[2k_2 + k_1 - 2v\left(k_2 - k_1\right)\right]}{2k_2 + k_1 + v\left(k_2 - k_1\right)} \tag{11}$$

Babanov [11]:

$$k_{eff} = \frac{k_2\left(k_2 + v^{2/3}\left(k_1 - k_2\right)\right)}{k_2 + v^{2/3}\left(k_1 - k_2\right)\left(1 - v^{1/3}\right)} \tag{12}$$

Brailsford [12]:

$$k_{eff} = \frac{1}{4}\left[\left(2-3v\right)k_2 + \left(3v-1\right)k_1 + \sqrt{8k_1k_2 + \left[\left(2-3v\right)k_2 + \left(3v-1\right)k_1\right]^2}\right] \tag{13}$$

2.5.2 Equivalent thermal expansion rate

Linear mixing rules [13]:

$$\alpha_c = \alpha_m V_m + \alpha_p V_p \tag{14}$$

Turner [14]:

$$\alpha_c = \frac{\alpha_m V_m K_m + \alpha_p V_p K_p}{V_m K_m + V_p K_p} \tag{15}$$

Kerner [15]:

$$\alpha_c = \alpha_m V_m + \alpha_p V_p + \left(\alpha_p - \alpha_m\right) V_m V_p \frac{K_p - K_m}{K_m V_m + K_p V_p + 3K_p K_m / 4G_m} \tag{16}$$

2.5.3 Equivalent elastic modulus

Dilute method:

$$\begin{cases} K_{eff} = K_m\left(1 + \dfrac{V_f\left(K_f / K_m - 1\right)}{1 + \left[\left(1+v_m\right)/3\left(1-v_m\right) - V_f\right]\left(K_f / K_m - 1\right)}\right) \\ G_{eff} = G_m\left(1 + \dfrac{V_f\left(G_f / G_m - 1\right)}{1 + \left[2\left(4-5v_m\right)/15\left(1-v_m\right) - V_f\right]\left(G_f / G_m - 1\right)}\right) \end{cases} \tag{17}$$

Self-consistent method [16]:

$$\begin{cases} K_{eff} = K_m + \dfrac{V_f K_{eff}\left(K_f - K_m\right)}{K_{eff} + \left[3K_{eff} / \left(3K_{eff} + 4G_{eff}\right)\right]\left(K_f - K_{eff}\right)} \\ G_{eff} = G_m + \dfrac{V_f G_{eff}\left(K_f - K_m\right)}{K_{eff} + \dfrac{16K_{eff} + 12G_{eff}}{15K_{eff} + 10G_{eff}}\left(G_f - G_{eff}\right)} \end{cases} \tag{18}$$

Mori-Tanaka [17]:

$$\begin{cases} K_{eff} = K_m \left(1 + \dfrac{V_f \left(K_f / K_m - 1 \right)}{1 + \alpha \left(1 - V_f \right) \left(K_f / K_m - 1 \right)} \right) \\ G_{eff} = G_m \left(1 + \dfrac{V_f \left(G_f / G_m - 1 \right)}{1 + \beta \left(1 - V_f \right) \left(G_f / G_m - 1 \right)} \right) \end{cases} \tag{19}$$

3 BEHAVIOR ANALYSIS CODE DEVELOPMENT

To accurately predict the performance of dispersion fuel plate, behavior analysis codes should be able to perform the thermal-hydraulic analysis, mechanic analysis and material property calculation, which are not isolated but coupling with each other with the consideration of burnup effects. Figure 3 presents the coupling scheme adopted in the code development. The followings were taken account into the investigation of influence caused by burnup effect: 1) the variations of thermal conductivity of fuel pellet and the geometric sizes due to the increasing burnup will affect the thermal performance of fuel plates; 2) the intrinsic strains caused by fuel densification and swelling worked as the driving force in mechanical deformation; 3) the irradiation will exert an substantial influence on the material properties, such as thermal conductivity, yield limit, Young modulus and shear modulus.

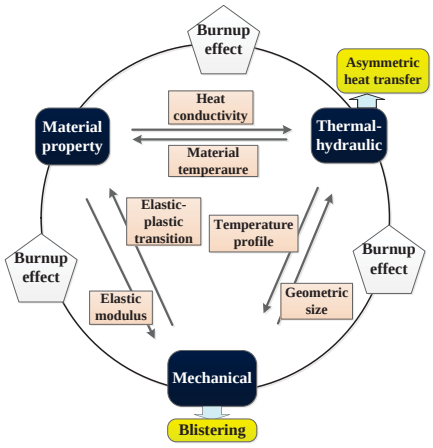

Figure 3. Coupling scheme of code

Based on the above physical models and coupling theory, the thermal-mechanical-material behavior coupling analysis code was developed by Fortran 90 with the consideration of burnup effects. After that, the time step sensitivity study for this code was performed. The result indicates that the time step should be much smaller (lower than two days) in the initial operation period (about 0 – 20 days) for undistorted simulation of densification while no substantial influence of time step on key parameters was found in subsequent operation stages. It also should be noted that if the time step is bigger than 30 days, there might be convergence problem in code calculation.

4 BEHAVIOR ANALYSIS AND DISCUSSION

A hypothetical plate-type fuel assembly was proposed as the subject investigated and its major geometric sizes and operating parameters were listed in table II. Based on the hypothetical assembly and the developed code, thermal-mechanical-material behavior analysis and blistering prediction was conducted.

Table II. Geometric sizes and operating parameters of the hypothetical assembly

Parameter	Value	Parameter	Value
Plate number	20	Channel number	21

Plate height	1000 mm	Plate width	80 mm
Plate thickness	2.8 mm	Cladding thickness	0.4 mm
Edge channel width	3 mm	Middle channel width	2 mm
Coolant pressure	6 MPa	Inlet temperature	513.15 K
Mass flow rate	18 kg/s	Assembly power	2 MW
Volume fraction of fuel	20%	Time step	20 days
Power distribution	Plates	The peak factor of the middle plate is 1.3	
	Axial direction (z)	Cosine distribution	
	Width direction (y)	Uniform distribution	
	Thickness direction (x)	Uniform distribution	

4.1 Thermal-hydraulic Results

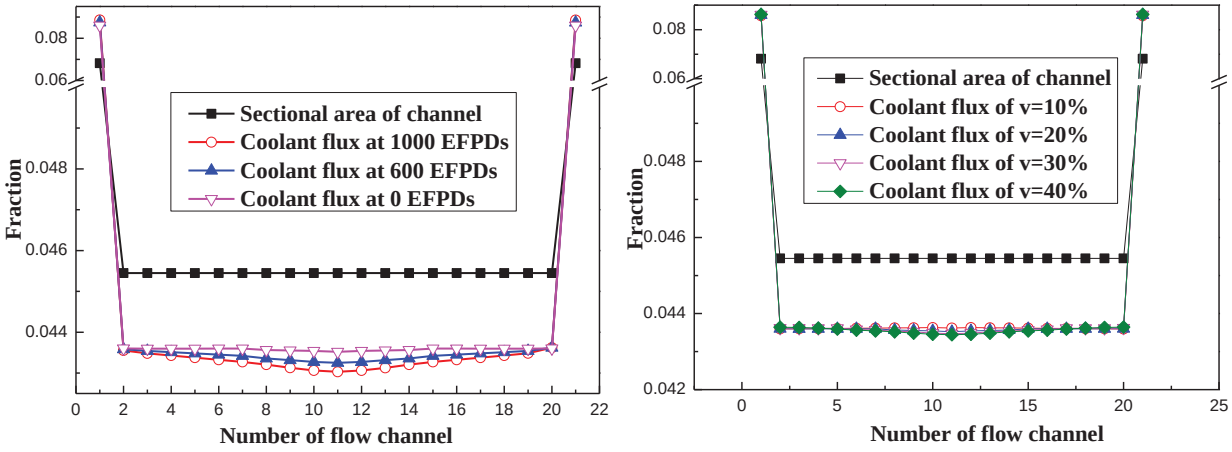

(a) Different burnup stages (b) Different volume fractions of UO_2

Figure 4. Coolant flux distribution

Figure 4 presents the coolant flux distribution of different channels. From the figure 4 (a), we can see that the coolant fractions in the two edge channels were much higher than that in middle channels. That was because the width of the edge channel was substantially larger than that of the middle channel. As the operating time increased, the coolant flux distribution changed slightly due to the geometric deformation. As shown in figure 4 (b), there is almost no difference between the coolant distributions when the fuel volume fraction increased, which indicates that the influence of power rise or decline can be neglected. So a conclusion might be drawn that the coolant flux distribution was determined mainly by the geometric condition.

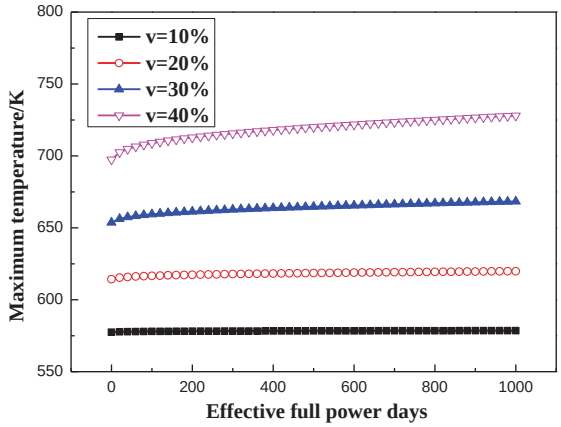

Figure 5. Temperature variation versus time

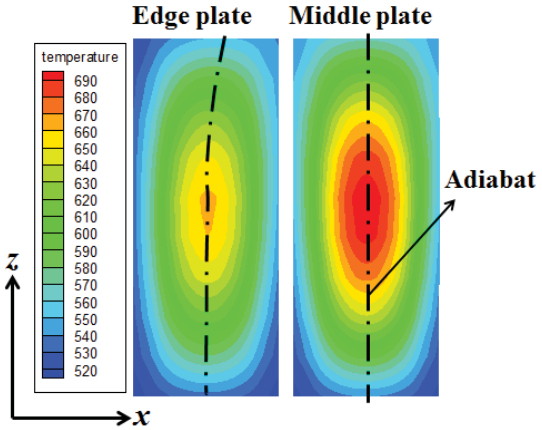

Figure 6. Temperature contour of plate

Figure 5 shows the maximum temperature variation versus operating time. Two substantial variation rules can be found: a) the temperature of dispersion plate-type fuel was much lower than temperature of the typical oxide ceramic fuel rod because of the higher heat conductivity, lower power density and shorter route of heat conduction in solid; b) during the whole operation, the fuel temperature changed slightly while more than 200 K temperature difference may exist in oxide fuel rod. That was because the heat conductivity change of UO_2 with burnup is much larger than that of Zr. In addition, the gas gap closure exerts a more substantial influence of heat transfer in fuel rod while there in no gas gap in plate-type fuel. Figure 6 presents the section temperature contours of the edge and middle plates. As shown in this picture, we can see that substantial asymmetric heat transfer occurred in edge plate due to the different channel widths at the two sides.

4.2 Mechanical Results

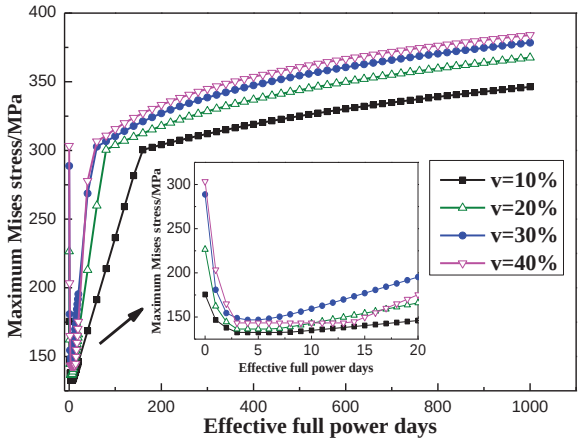

Figure 7. Maximum stress variation versus time

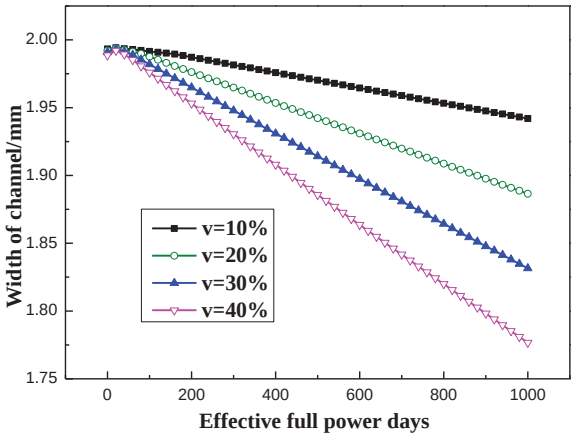

Figure 8. Channel width variation versus time

The maximum equivalent stress variation versus operating time was presented in figure 7. The variation regulations can be found that the Mises stress decreased rapidly first and then increased rapidly to about 300 MPa (yield stress). After that, the stress increased slightly. The Mises stress drop at the initial stage was caused by the fuel densification which will offset the action of thermal expansion. When the densification was completed, the radiation swelling started to play the dominant role. After yield, the matrix material entered into plastic stage and the stress increased slowly with the rapidly increasing strain. Figure shows the channel width variation versus time. As shown in this figure 8, if the fuel volume fraction and burnup are enough high, the channel width might undergo a substantial decrease (up to 10%) due to the thermal expansion and burnup effects of fuel plate, which might exert a bad influence on heat transfer.

4.3 Blistering Prediction

As a particular failure mode for dispersion plate-type fuel, blistering results in deterioration of heat transfer in the core and over plastic deformation of cladding which might lead to cladding break and fission gas leak. Many investigators have devoted themselves to annealing experiments to obtain the threshold temperature of blistering. In this study, mechanism study was conducted aiming to simulate blistering processes and predict the start time of blistering by numerical approach.

4.3.1 Mechanism of blistering

In this paper, blistering was divided into five stages: fission gas generation and bubble growth, bubble break and gas release, matrix damage and break, free gas accumulation in free space, gas pressure rise and blistering.

1. Fission gas generation and bubble growth: every fission reaction generates about 31 gas molecules. Most of fission gases are insoluble in fuel pellet and gathered in UO_2 crystals resulting in bubbles which grow with the increasing burnup.

2. Bubble break and gas release: with the increasing bubble size and pressure, gas bubbles will break at a certain burnup. The mathematic expression for prediction of bubble break is [18]:

$$p > 2\gamma / R + \sigma \tag{20}$$

where p presents the gas pressure, γ (about 1 N/m) presents solid tension of UO_2, R is the bubble radius and σ presents the hydrostatic pressure which can be 20-250 MPa in UO_2. After bubble break, the fission gas will be released to the free space in UO_2 sphere pellets. The fission gas release calculation can consult relevant literatures [19-21].

3. Matrix damage and break: The equivalent stress of fuel plate increased due to the thermal expansion and swelling and might up to the yield stress at a certain burnup. The stain of matrix metal increased rapidly in plastic stage, which finally results in matrix damage and break. The equivalent stress calculation has already been introduced in preamble.

4. Free gas accumulation in free space: after matrix damage and broken, the broken crack of matrix results in certain free space which was connected with the free space in fuel pellets. So the fission gas contained in fuel pellets flowed to matrix broken cracks. With the reactor operation, more fission gas was released and accumulated in the free space.

5. Gas pressure rise and blistering: At a certain operation time, the broken crack at some local area extended to the whole plate in thickness direction (y direction) and the released fission gas can arrive at the interface of the cladding and the pellet. After that, no more cracks were generated while fission gases was still produced and released at the local place, which resulted in a pressure rise. There might be some defects in some places of cladding, where the capacity to resist mechanical deformation was not as good as that in other places. When the gas pressure up to a certain value, plastic deformation might occur at the cladding having defects and blistering happened. Figure 9 shows the force schematic diagram of blistering.

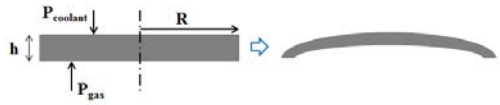

Figure 9. Force schematic diagram of blistering

The criterion for blistering judgment is that the maximum stress in cladding is larger than the local yield stress ($\sigma^{max} \geq \sigma_{yield}$). The maximum stress in cladding can be obtained by analytical method:

$$\sigma^{max} = \frac{3(P_{gas} - P_{coolant})R^2}{4h^2} \tag{21}$$

4.3.2 Prediction results

Figure 10 presents the blistering start time. As shown in figure 10 (a), the plate with a larger volume fraction of UO2 was subjected to blistering substantial earlier than the plate with less UO2 fuel. The reason to explain this is that more fuel generates more fission gases. Furthermore, the higher cladding temperature caused by the higher power will substantially reduce the yield stress. From figure 10 (b), we can see that blistering was sensitive to cladding thickness. If the thickness increased from 0.4 mm to 0.8

mm, it can be guaranteed that blistering will not occur before 800 EFPDs, which might provide some inspirations for prevention or delay of blistering fail.

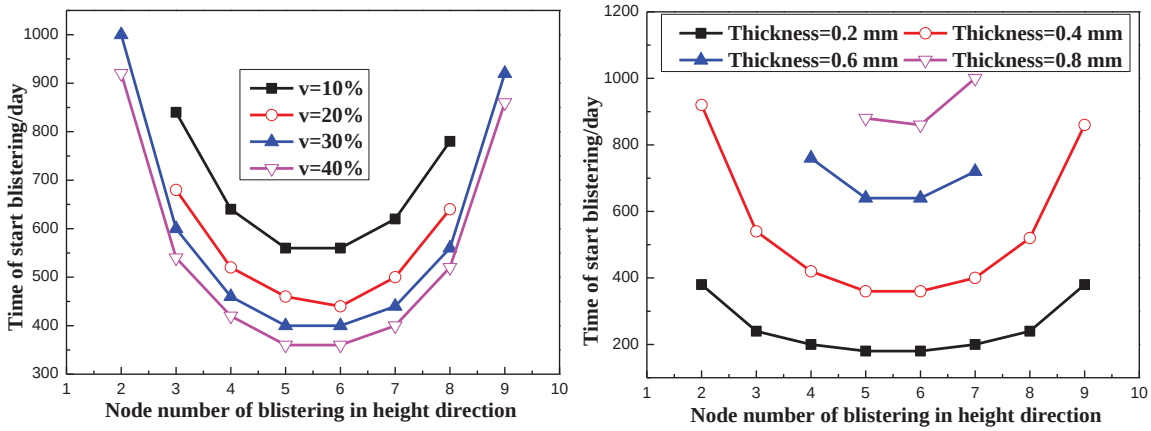

(a) Different volume fractions of UO_2 (b) Different thicknesses of cladding

Figure 10. Blistering prediction

5 CONCLUSIONS

In this paper, a thermal-mechanic-material coupling analysis code was developed to perform the behavior analysis of a hypothetical plate-type fuel assembly and the following conclusions can be drawn:

1. Geometric section of the flow channel plays the decisive role in coolant flux distribution. The temperature of plate-type fuel is much lower than that of oxide fuel rods and changes slightly during the operation. The temperature profile of the edge plate indicates that substantial asymmetric heat transfer occurred caused by the asymmetric geometry
2. Fuel densification and radiation swelling respectively plays the dominant role in Mises stress variation at the initial burnup stage and the subsequent phase. The matrix material will undergo substantial plastic deformation which resulted in matrix damage and significant width change of channels.
3. As the fission gas releasing, blistering might happened at the cladding with defects, which cause the mechanical and thermal failure. Increasing the cladding thickness might be one of the effective measures to prevent or delay blistering.

6 ACKNOWLEDGMENTS

This study was supported by Key Laboratory of Nuclear Reactor System Technology Design.

7 REFERENCES

1. K. J. Geelhood, W.G. Luscher, "FRAPCON-3.5: A Computer Code for the Calculation of Steady-State Thermal-Mechanical Behavior of Oxide Fuel Rods for High Burnup," *NUREG/CR-7022*, **v1**, pp.1-152 (2014).
2. K. J. Geelhood, W.G. Luscher, J. M. Cuta, "FRAPTRAN-1.5: A Computer Code for the Transient Analysis of Oxide Fuel Rods," *NUREG/CR-7023*, **v1**, pp.1-217 (2014).
3. D. L. Keller, "Predicting burnup of stainless-UO_2 cermet fuels," *Nucleonics*, **19(6)**, pp.45-48 (1961).
4. R. J. Scavuzzo, "Structural analysis of fuel growth in fuel plates," *Nuclear Engineering and Design*, **3**, pp.199-203 (1966).

5. Chenetal N. C. J, “Conceptual Design Loss-Of-Coolant Accident Analysis for The Advanced Neutron Source Reactor,” *Nuclear Technology*, **11**, pp.105-114 (1994).
6. Chao J, “COBRA 3C/RERTR: A thermal-hydraulic subchannel code with low pressure capabilities,” *Argonne National Laboratory*, (1980).
7. Chen J. C, “Correlation for Boiling Heat Transfer to Saturated Fluids in Convective Flow,” *Industrial & Engineering Chmistry Process Design and Development*, **5(3)**, pp.322-328 (1966).
8. L. Prandtl, “Spannungsverteilung in plastischen,” *1st Int. Congr. Appl. Mech*, pp.43–46 (1924).
9. A. Reuss, “Ber¨ucksichtigung der elastischen Form¨anderung in der Plastizit¨atstheorie,” *Math. Mech*, **10**, pp.266–274 (1930).
10. J. C. Maxwell, *A treatise on electrictity and magnetism*, Oxford: Clarendon Press, London, British (1873).
11. A. A. Babanov, “Method of calculation of thermal conduction coefficient of capillary porous material,” *Sov. Technol. Phys*, **2**, pp.476-484 (1957).
12. A. D. Brailsford, “Thermal conductivity of aggregates of several phase, including porous materials,” *Br. J. Appl. Phys*, **15**, pp.313-319 (1964).
13. L. Geiger, M. Jackson, “Low-expansion MMCs boost avionics,” *Advanced Materials Process*, **136**, pp.23-28 (1989).
14. P. S. Turner, “Thermal expansion stress ini reinforced plastics,” *J Res Natl Bureau Standards*, **37**, pp.239-250 (1946).
15. E. H. Kerner, “The elastic and thermo-elastic properties of composite media,” *Proceedings of the Physical Society*, **69**, pp.808-813 (1956).
16. Hill R, “Theory of mechanical properties of fibre-strengthened materials self-consistent model,” *J Mech Phys Solids*, **13**, pp.189-198 (1965).
17. Benseniste Y, “A new approcach to the application of Mori-Tanaka’s theory in composite materials,” *Mech Materials*, **6**, pp.147-157 (1987).
18. Donald R. Olander, *Fundamental aspects of nuclear reactor fuel elements*, Energy Research and Development Administration, USA (1976).
19. Lee C. B, Yang Y. S., Kim D. H., “A New Mechanistic and Engineering Fission Gas Release Model for a Uranium Dioxide Fuel,” *Journal of Nuclear Science and Technology*, **45**, pp.60-71 (2008).
20. Bernard, L. C., Bonnaud, E, “Finite volume method for fission gas release modeling,” *Journal of Nuclear Materials*, **244**, pp.75-84 (1997).
21. Shohei U, Junya S, Koichi E, “Fuel and Fission Gas Behavior during Rise-to-power Test of the High Temperature Engineering Test Reactor(HTTR),” *Journal of Nuclear Science and Technology*, **40**, pp.679-686 (2003).